Reactions induced by the halo nucleus ^{6}He at energies around the Coulomb barrier

A. Di Pietro,[1,*] P. Figuera,[2] F. Amorini,[2,3] C. Angulo,[4] G. Cardella,[2] S. Cherubini,[5,†] T. Davinson,[1] D. Leanza,[2,3] J. Lu,[2] H. Mahmud,[1] M. Milin,[6] A. Musumarra,[2,3] A. Ninane,[5] M. Papa,[2] M. G. Pellegriti,[2,3] R. Raabe,[7] F. Rizzo,[2,3] C. Ruiz,[1,‡] A. C. Shotter,[1,§] N. Soić,[6] S. Tudisco,[2,3] and L. Weissman[7,‖]

[1]*School of Physics, University of Edinburgh EH9 3JZ Edinburgh, United Kingdom*

[2]*INFN Laboratori Nazionali del Sud and Sezione di Catania, I95123 Catania, Italy*

[3]*Universita' di Catania, I95125 Catania, Italy*

[4]*Centre de Recherches du Cyclotron, Chemin du Cyclotron 2, B1348 Louvain-la-Neuve, Belgium*

[5]*Institut de Physique Nucléaire and Centre de Recherches du Cyclotron, University of Louvain B1348 Louvain-la-Neuve, Belgium*

[6]*Ruđer Bošković Institute, 10002 Zagreb, Croatia*

[7]*Instituut voor Kern-en Stralingsfysica, University of Leuven, B3001 Leuven, Belgium*

(Received 2 December 2003; published 26 April 2004)

The reaction ^{6}He + ^{64}Zn was studied in order to investigate the effects of the projectile neutron-halo structure on the reaction mechanism at energies around the Coulomb barrier. Elastic scattering angular distributions, transfer/breakup angular distributions, and fusion excitation functions have been measured. Due to the low-recoil energy of the evaporation residues and the low intensity of the ^{6}He beam, the fusion cross section was measured by detecting off-line the atomic x-ray emission which follows the electron capture decay of the evaporation residues. For comparison the reaction ^{4}He + ^{64}Zn was studied using the same technique. The data for the reaction ^{6}He + ^{64}Zn show that the transfer and breakup mechanisms account for almost 80% of the total reaction cross section, moreover we do not observe an enhancement of the fusion cross section when compared with the ^{4}He + ^{64}Zn reaction.

DOI: 10.1103/PhysRevC.69.044613 PACS number(s): 25.60.Bx, 25.55.Ci, 25.60.Dz, 25.60.Pj

I. INTRODUCTION

In the past few years, in different laboratories, a great experimental effort has been devoted to studying reactions induced by radioactive beams in order to investigate the effects of nuclear structure on reaction mechanisms. In particular, both theoretical and experimental work have studied the effects of the halo structure of nuclei on the fusion reaction mechanism at energies near and below the Coulomb barrier.

Contradictory effects on fusion cross section have been predicted by different theoretical models in reactions induced by neutron-halo nuclei at energies around and below the Coulomb barrier. These models agree that the larger spatial extent of halo nuclei, and the coupling with possible low-lying resonant states, would increase the fusion cross section. However, the models disagree about the role played by the breakup of the loosely bound halo nucleons on the fusion cross section. Breakup could produce a loss of flux from the fusion channel and thus hinder the cross section [1–3]. Conversely, strong coupling with the breakup channel with the associated dynamical modulation of the fusion potential, could produce an enhancement of the sub-barrier fusion cross section [4]. At energies above the barrier, according to Ref. [4], the strong coupling with the breakup channel has the opposite effect of reducing the fusion cross section.

Experimental investigation is quite difficult due to the low intensity of radioactive beams (three or four orders of magnitude lower than typical stable beams) coupled with the small fusion cross sections at sub-barrier energies. To our knowledge, only three systems have been studied: ^{6}He + ^{209}Bi [5–8], ^{6}He + ^{238}U [9,10], and ^{11}Be + ^{209}Bi [11,12]. The ^{6}He + ^{209}Bi fusion reaction around and below the barrier leads to the production of heavy evaporation residues (E.R.) unstable against α emission. The fusion cross section was obtained by detecting the α particles following the E.R. decay. The authors found an enhancement of the fusion cross section below the barrier and a strong contribution due to the transfer and/or breakup reaction channels [5–8]. In the ^{6}He + ^{238}U system fusion reactions lead to fission of the compound nucleus. The fusion cross section was obtained from the detected fission events assuming that no significant contribution came from other reaction mechanisms. Once more, a large enhancement of the fusion cross section below the barrier was observed [9,10]. In the ^{11}Be + ^{209}Bi system the cross section was obtained by detecting α particles emitted in the E.R. decay. However, in contrast to the previous two systems, no enhancement was observed. In fact, similar fusion cross sections have been measured for the ^{9,11}Be + ^{209}Bi reactions at energies below the Coulomb barrier [11], whereas a larger fusion cross section was found above the barrier for the halo nucleus induced reaction. However, in the ^{11}Be + ^{209}Bi experiment the fusion cross section was obtained by summing the contribution of the $5n, 4n$, and fission channels, the $3n$ channel was not measured. This channel is expected to be relevant below the barrier. Conversely the fis-

*Present address: INFN-Laboratori Nazionali del Sud, Catania, Italy.

†Present address: Ruhr University, Bochum, Germany.

‡Present address: TRIUMF, Vancouver, British Columbia, Canada.

§Present address: TRIUMF, Vancouver, British Columbia, Canada.

‖Present address: NSCL, Michigan State University, East Lansing, Michigan.

sion cross section below the barrier could have been overestimated [11,13].

The ^{9}Be nucleus being weakly bound ($S_n = 1.6$ MeV) may not be the best reference nucleus to compare the fusion cross section with. In fact a reduction of the fusion cross section above the barrier was found in the ^{9}Be + ^{208}Pb [14,15] reaction, and data on ^{9}Be + ^{209}Bi show a large transfer/breakup cross section below the barrier [13] as in ^{6}He + ^{209}Bi [8,16].

The effects of projectile structure on reaction mechanisms seem also to depend on the target mass. In fact, contrary to the above mentioned ^{9}Be + ^{208}Pb case [14], no effects on fusion cross section were found for ^{9}Be + ^{64}Zn at near barrier energies [17]. The fusion cross section in this case was the same as for reactions induced by tightly bound nuclei.

In summary, the existing experimental data give apparently contradictory results and more data are necessary to better understand the problem. We note, in addition, that the two experimental techniques mentioned above can be applied only to heavy systems leading to fission or α unstable evaporation residues.

We have measured ^{6}He induced reactions on a medium mass ^{64}Zn target at energies around the Coulomb barrier. We used an experimental setup suitable for the study of the fusion process and the other open channels: elastic, transfer, and breakup.

To our knowledge, no data for fusion reactions induced by neutron-halo nuclei on medium mass targets around the barrier are available. To overcome the experimental difficulties of measuring low-energy fusion cross sections induced by low-intensity beams, we measured off-line the atomic X-ray emission following the electron capture (E.C.) decay of the E.R. produced in the reaction. The choice of ^{64}Zn as a target was made, with the help of statistical model calculations, in order to have the largest fraction of the fusion cross section producing radioactive E.R. mainly decaying by E.C. The fusion excitation function was performed at a fixed beam energy using the activation technique. For comparison, the reaction ^{4}He + ^{64}Zn was also measured at the same center of mass (c.m.) energy.

In Sec. I we will describe the experimental techniques, in Sec. II the results for the different channels (elastic scattering, transfer/breakup, fusion) will be presented, and Sec. III will be dedicated to final remarks and conclusions.

II. EXPERIMENTAL TECHNIQUES

A. Detector setup

The experiment was performed at the Centre de Recherches du Cyclotron at Louvain la Neuve with an average ^{6}He beam current of 3×10^{6} pps. A total of two runs were performed. In the first run we measured the reaction ^{6}He + ^{64}Zn at $E_{\rm lab} = 10$ MeV. A 1 mg/cm^2 self-supporting ^{64}Zn target was used. The experimental setup is shown in Fig. 1(a) and consisted of three arrays of highly segmented, large solid angle Si strip detectors covering a total solid angle $\Omega \approx 2\pi$. The detectors used were 20 sectors of the Louvain la Neuve-Edinburgh-detector-array (LEDA) [18] with a total of 320 strips. The first array LEDA consisted of eight sectors, placed in an annular configuration with each sector normal to the beam direction. The laboratory angular range covered was $0° \leqslant \phi \leqslant 360°$ and $5° \leqslant \theta \leqslant 12°$. The other two arrays each consisted of six sectors at 45° with respect to the beam axis and covering the laboratory angular ranges $20° \leqslant \theta \leqslant 65°$ and $120° \leqslant \theta \leqslant 160°$ respectively, with $0° \leqslant \phi \leqslant 360°$. The configuration of these two detector arrays is called LAMP due to its lampshade shape and it allows for a very large solid angle coverage.

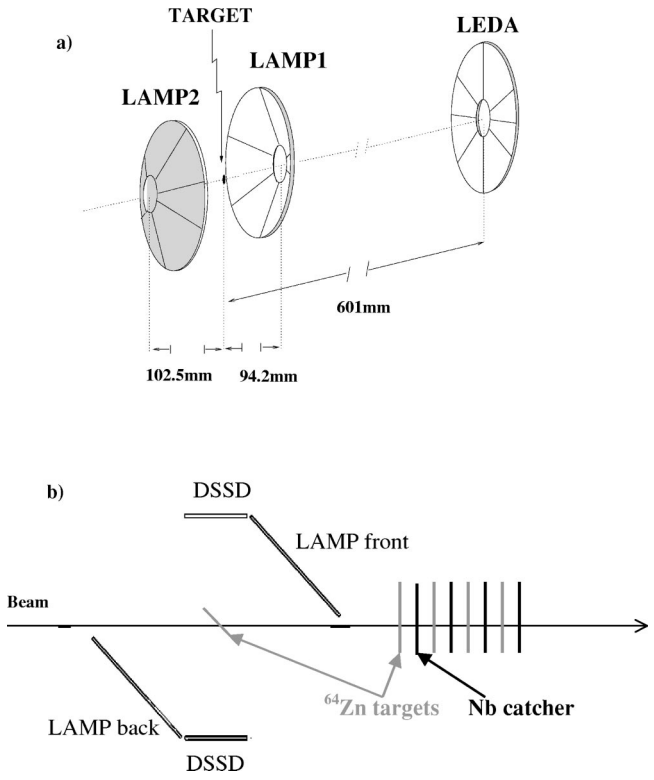

FIG. 1. Schematic diagram of the experimental setup: (a) for the run at $E_{\rm lab} = 10$ MeV; (b) for the run at $E_{\rm lab} = 13.6$ MeV. See text for details.

In this run only light charged particles such as p, α, and ^{6}He were detected. Hydrogen was discriminated from He by means of the time of flight (ToF) technique using the cyclotron rf as the time reference.

In the second run the same reaction was measured at $E_{\rm lab} = 13.6$ MeV and, as a comparison, the reaction ^{4}He + ^{64}Zn was also measured at the same c.m. energy ($E_{\rm c.m.} = 12.4$ MeV). The experimental setup used in this run was modified in order to have a more complete angular coverage and it is sketched in Fig. 1(b). The target was a 0.5 mg/cm^2 self-supporting ^{64}Zn foil. It was angled at 45° with respect to the beam direction in order to measure at laboratory angles around 90°. The detectors used were two halves of a LAMP detector array, one at forward and one at backward angles, each consisting of three sectors covering the laboratory angular range $0° \leqslant \phi \leqslant 180°$ and $15° \leqslant \theta \leqslant 50°$ (LAMP front) and $180° \leqslant \phi \leqslant 360°$ and $120° \leqslant \theta \leqslant 160°$ (LAMP back). Four double sided silicon strip detectors [18] covered the angular range $70° \leqslant \theta \leqslant 100°$. Two were placed above and two below the target position as shown in Fig. 1(b). This detector geometry allowed for a very large angular coverage with good granularity. A total of 240 strips were used. In this

run hydrogen was also discriminated from helium using the ToF technique.

With this setup the elastic scattering and light charged particle angular distributions were measured. As sketched in Fig. 1(b), downstream of the primary ^{64}Zn target, in a cube adjacent to the scattering chamber containing the Si detector arrays, we placed a stack of four ^{64}Zn foils alternated with ^{93}Nb catcher foils which were used for the activation experiment. This will be discussed in detail in the following section.

B. Activation experiment

A fusion reaction induced by a beam of light halo nuclei on a medium mass target, at energies around and below the barrier, will lead to production of low-energy evaporation residues which are stable against α decay. Therefore none of the techniques previously used [6,9,11] is suitable for studying such reactions. Direct E.R. detection will be very difficult since, typically, the slow E.R. will be in the same energy range as the β background from the decay of the scattered radioactive beam. Moreover a fraction of the E.R. produced will not come out from the target since their energies are too small. For example, in the present experiment for a ^{6}He beam of 13.5 MeV and a ^{64}Zn target having a thickness of 2 mg/cm^2 the fraction of E.R. stopped inside the target is about 80%. On the other hand indirect E.R. detection via on-line or off-line gamma spectroscopy techniques, is very difficult due to the high background compared to the low E.R. yields and to the low Ge detector efficiencies. To overcome these difficulties we decided to measure off-line the x rays following the E.C. decay of the E.R. to study the fusion reactions ^{4,6}He+^{64}Zn. This technique can be used by choosing, with the help of statistical model calculations, a suitable target such that all (or at least a large fraction) of the possible E.R. produced are unstable against E.C. decay. The main advantages of the proposed technique are the following.

(a) Atomic x rays in the energy region of interest (5–10 keV) can be easily detected off-line with extremely low background and 100% intrinsic detection efficiency by using Si(Li) detectors.

(b) The E.R. can be identified by atomic number from the energy of the x-ray lines, whereas different isotopes can, in some cases (as in the present case), be separated by their half lives.

(c) By activating a stack of targets it is possible to extract the cross section at different energies without changing the beam energy thus reducing the beam time needed to perform an excitation function measurement with the very low intensity radioactive beams.

As previously mentioned, a stack of four ^{64}Zn targets ($\sim$2 mg/cm^2 thick) followed by ^{93}Nb catchers ($\sim$3 mg/cm^2 thick) were placed about 70 cm downstream of the thin ^{64}Zn "scattering" target. The catchers were needed in order to stop the residues emerging from the previous target and to slow down the beam, increasing the average difference in beam energy for the different targets. Using these stacks, we explored a center of mass energy range 8 MeV$\leqslant E_{\mathrm{c.m.}} \leqslant$12 MeV in the ^{6}He induced reactions and 10 MeV $\leqslant E_{\mathrm{c.m.}} \leqslant$12 MeV in the ^{4}He case (only three targets were used). The error in determining the beam energy at the center of each target in the stack is due to the error in the target thickness and in the stopping power since different programs give slightly different stopping power values. Since the target thickness was measured by the energy loss of 5.48 MeV α particles traversing the foil, the source of error is due to the energy loss calculations. The error in the calculations was estimated by using several energy loss programs which gave a maximum difference of 3%. Of course, the error in the energy loss in each foil must be considered, therefore the largest error in the beam energy occurs at the last target of the stack and is about ±150 keV. The energy loss program used for our calculations was SRIM [19].

Different activation runs were performed with ^{6}He beams to optimize the production of short lived and long lived residues. x rays emitted from the different targets (together with the corresponding catcher) were measured off-line using ORTEC Si(Li) detectors surrounded by lead shields. Possible reactions induced by the beam on the ^{93}Nb catchers do not represent a problem since the x ray energies are different to the ones corresponding to reactions on ^{64}Zn. Due to the very low background, we were able to measure low counting rates which were, in some cases, of the order of 1 count/h.

The beam current was determined from the elastic scattering at small angles where the elastic cross section is known to be Rutherford. To extract the cross sections for the production of various residues, especially for short-lived nuclides, it was necessary to monitor the beam current as a function of time, during the activation run. In order to do this, a clock signal was generated by using the signal of a pulse generator with a fixed (and stable) frequency. This signal was stored on tape along with the elastic scattering data. A spectrum, time versus counts in the elastic peak at small angles was extracted from the data with a 1 min time bin and, after normalization, the incident current as a function of time was obtained.

The x-ray activity emitted by each ^{64}Zn foil was measured by placing both the ^{64}Zn target and the ^{93}Nb catcher very close to the Si(Li) detector. The ^{93}Nb foil was placed on top of the ^{64}Zn foil so that they were measured simultaneously. Each measurement was repeated in order to measure the activity as a function of time. The average x-ray absorption by the ^{64}Zn and ^{93}Nb foils has been estimated with the help of a Monte Carlo statistical model calculation [20] that calculates the E.R. energy spectra and implantation profile within the target. In these calculations the reaction could take place randomly within the ^{64}Zn target. This self-absorption is different for the different x-ray lines, with an average value of about 6.5%.

The incident beam profile was measured in order to extract the Si(Li) geometric detection efficiency. The beam profile along with the detection geometry were folded into a Monte Carlo code. The extracted total efficiency was 2.1%.

III. EXPERIMENTAL RESULTS

A. Elastic scattering

The elastic scattering angular distributions were extracted for all of the reactions studied. In Fig. 2(a) a comparison

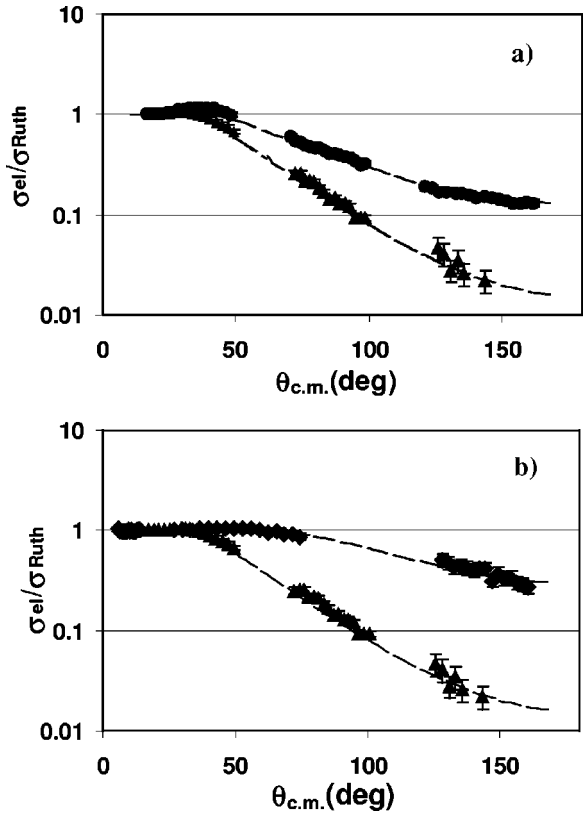

FIG. 2. (a) Elastic scattering angular distributions at $E_{\text{c.m.}}=12.4$ MeV for ^{4}He+^{64}Zn (closed circles) and ^{6}He+^{64}Zn (closed triangles). (b) Elastic scattering angular distributions for ^{6}He+^{64}Zn at $E_{\text{c.m.}}=9$ MeV (closed diamonds) and $E_{\text{c.m.}}=12.4$ MeV (closed triangles). The dashed lines represent the results of the corresponding optical model fits.

between the elastic scattering angular distributions for the two reactions ^{4}He+^{64}Zn and ^{6}He+^{64}Zn at the same c.m. energy ($E_{\text{c.m.}}=12.4$ MeV) is shown. As one can see from this comparison there is much more flux removed from the elastic channel in the reaction induced by the halo nucleus ^{6}He than there is with the stable nucleus ^{4}He. This implies a much larger reaction cross section (more than a factor 2 larger) for the ^{6}He induced reaction. In Fig. 2(b) the elastic scattering angular distributions for ^{6}He+^{64}Zn at $E_{\text{lab}}=10$ MeV ($E_{\text{c.m.}}=9$ MeV) and $E_{\text{lab}}=13.6$ MeV($E_{\text{c.m.}}=12.4$ MeV) are shown.

An optical model χ^2 analysis was performed on the elastic scattering data using the code PTOLEMY [21]. The details of the light charged particle analysis are reported in Ref. [22], and we will only summarize the results here. The real and imaginary part of the optical potential used in the calculations were Wood-Saxon wells. The ^{6}He+^{64}Zn data at the two beam energies were fitted using as free parameters the real and imaginary potential depths. To avoid a fit with many free parameters all other parameters were fixed. For the optical model χ^2 analysis of the reaction ^{4}He+^{64}Zn at ($E_{\text{c.m.}}=12.4$ MeV) we followed the same procedure as in the ^{6}He+^{64}Zn case. α particle scattering on heavy target is known to have continuous ambiguities of the Igo type [23]. In this case a similarly good fit was obtained with a much larger real potential depth and smaller radius. We also verified that the addition of a surface-derivative type potential to the volume part of the imaginary potential did not improve the fits. The values of the optical model parameters obtained from the fits are shown in Table I and the results of the fit are shown in Figs. 2(a) and 2(b). From the optical model analysis of elastic scattering data the total reaction cross sections were extracted. We obtained the following values: for ^{4}He+^{64}Zn $\sigma=(650\pm80)$ mb at ($E_{\text{c.m.}}=12.4$ MeV) and for ^{6}He+^{64}Zn $\sigma=(380\pm60)$ mb and (1450 ± 130) mb at $E_{\text{c.m.}}=9$ and 12.4 MeV, respectively. As we will see in the following the largest fraction of the total reaction cross section in the ^{6}He case corresponds to transfer/breakup events.

TABLE I. Optical model parameters.

Reaction	$E_{\text{c.m.}}$(MeV)	V	r_0	a	W	r_i	a_i
^{4}He+^{64}Zn	12.4	123	1.2	0.43	20.4	1.05	0.43
^{6}He+^{64}Zn	12.4	104	1.2	0.6	38.9	1.2	0.85
^{6}He+^{64}Zn	9.1	47.4	1.2	0.6	10.7	1.2	0.85

B. Transfer and breakup channels

In the experiment ^{6}He+^{209}Bi a very large cross section (almost saturating the total reaction cross section) due to transfer and/or breakup was found [7,8]. In our data we also looked for such events. Figure 3 shows an energy spectrum at $\theta=90°$ for the reaction ^{6}He+^{64}Zn at $E_{\text{lab}}=13.6$ MeV obtained by gating on the helium locus in the ToF-energy spectrum. One can see that there is a strong α-particle contribution in addition to the ^{6}He elastic scattering peak. As discussed in Ref. [22], α particles are expected to be produced in fusion evaporation, one and two neutron transfer

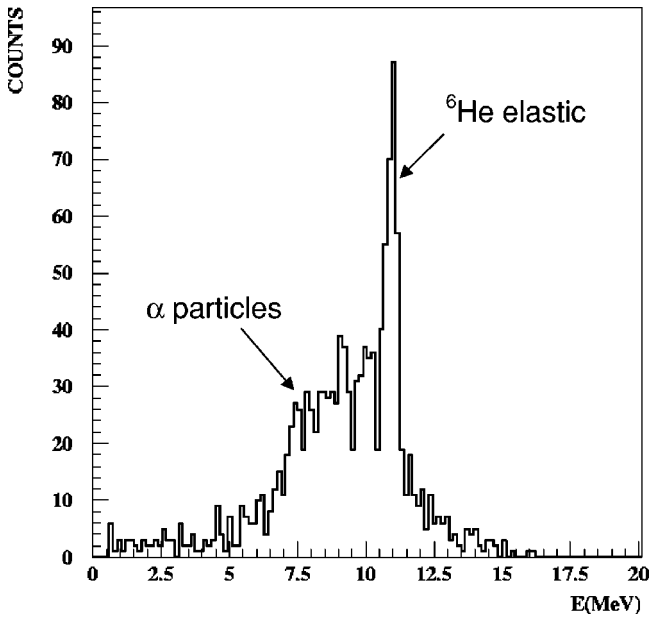

FIG. 3. Energy spectrum of α and ^{6}He locus measured at $\theta_{\text{lab}}=90°$ for the reaction 13.6 MeV ^{6}He+^{64}Zn.

and breakup processes. In general, different mechanisms can be discriminated by their energy and/or angular distributions. However, in the present case it is not easy to distinguish different reaction channels based upon energy considerations alone [16]. Different mechanisms will, in fact, produce events in approximately the same energy region. One or two neutron transfer to the ground state is not likely to occur since the optimum Q-value for neutron transfer is $Q_{\mathrm{opt}} \sim 0$. In fact no events in the energy region corresponding to $2n$ transfer ($Q_{\mathrm{g.s.}} = 18.06$ MeV) to the ground state are present. One neutron transfer ($Q_{\mathrm{g.s.}} = 6.11$ MeV) produces ^{5}He which then decays to ^{4}He$+1n$. The energy region for the α-particles from one and two neutron transfer is slightly different but, as shown in Fig. 3, it is not possible from the energy spectrum to distinguish the two transfer processes since the experimental energy distribution is quite broad. A possible way to discriminate α particles from direct (transfer and/or breakup) or fusion reactions is the angular distribution. Evaporated α particles are expected to be produced with an almost isotropic angular distribution since they are emitted from a compound nucleus having very small velocity and low angular momentum [$J_{\mathrm{max}} \sim 5\hbar$ for $E_{\mathrm{lab}}(^6\mathrm{He}) = 13.6$ MeV as predicted by CASCADE [24]]. The α particle angular distribution for transfer and breakup channels is expected to be peaked, typical of direct processes with a maximum in the angular distribution that moves to larger angles as the beam energy decreases.

The α particle angular distributions for ^{6}He$+^{64}$Zn were obtained by subtracting the elastic scattering contribution with a two Gaussian fit. They are shown in Figs. 4(a) and 4(b) at $E_{\mathrm{lab}} = 10$ and 13.6 MeV, respectively. Small angles ($\theta \leqslant 30°$) were not considered since the elastic scattering contribution was too strong to be subtracted. It seems evident from the angular distributions that the dominant mechanisms are transfer and/or breakup. However a small contribution due to inelastic scattering cannot be excluded.

The integrated α particle cross sections are (300 ± 100)mb and (1200 ± 150)mb at $E_{\mathrm{lab}} = 10$ and 13.6 MeV, respectively. From the comparison of these cross sections with the reaction cross sections extracted from elastic scattering, one can see that the largest fraction of the reaction cross section (about 80%) corresponds to transfer and breakup channels. This result is in agreement with Ref. [7] for the reaction ^{6}He$+^{209}$Bi. As discussed in Ref. [22], transfer processes have been identified by looking at events where the α particle was detected in coincidence with protons or another α particle. In Fig. 5 we show an energy spectrum of protons and α for the reaction ^{6}He$+^{64}$Zn at $E_{\mathrm{lab}} = 10$ MeV with the condition of a charged particle multiplicity of two. A peak at $E \sim 6.5$ MeV is evident in the spectrum. The peak position moves with angle and, according to kinematical calculations, it corresponds to α particles emitted after $2n$ transfer to form ^{66}Zn*. The $1n$ transfer channel cannot contribute to the peak since the excitation energy, owing to the smaller $Q_{\mathrm{g.s.}}$, is not sufficient for charged particle emission from ^{65}Zn* (notice that we are looking at events having charged particle multiplicity 2). Not only α-p and α-α events can be produced in $2n$ transfer reactions but also α-n which cannot be detected in the experiment but can contribute to the production of ^{65}Zn. As will be discussed in the following, strong production of ^{65}Zn has been observed within the activated targets which further confirms a strong contribution by the transfer process.

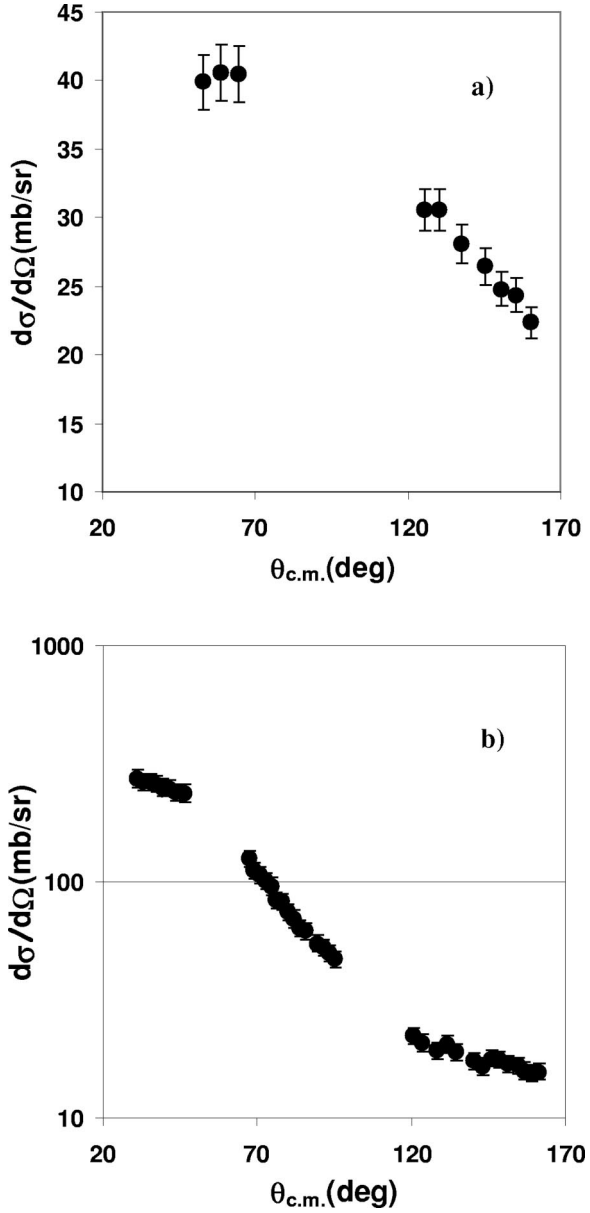

FIG. 4. (a) α particle angular distribution for ^{6}He$+^{64}$Zn at $E_{\mathrm{c.m.}} = 9$ MeV. (b) α particle angular distribution for ^{6}He$+^{64}$Zn at $E_{\mathrm{c.m.}} = 12.4$ MeV.

C. Fusion excitation function

The fusion excitation function was extracted by measuring the contribution of each radioactive E.R. produced in the reaction. In fact statistical model calculations performed with CASCADE predict that the contribution of stable E.R. is, at most, 3% of the total cross section. As we will see in the following, the extracted E.R. cross section agrees rather well with the CASCADE predictions with the exception of one nuclide, ^{65}Zn.

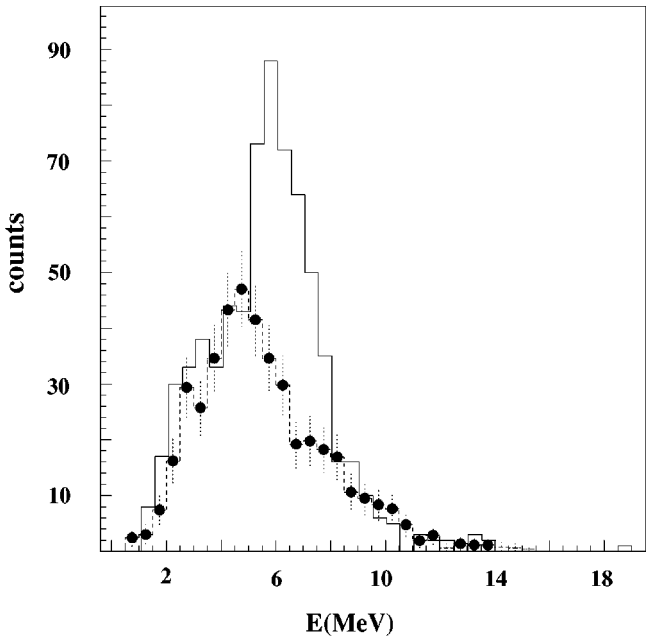

FIG. 5. Energy spectrum of events with charged particle multiplicity 2 at backward angles for the run at $E_{\mathrm{c.m.}}=9$ MeV. The symbols represent the contribution of fusion evaporation events calculated using a Monte Carlo statistical code.

Typical yields of x rays measured off-line for the reaction ^{6}He+^{64}Zn are shown in Figs. 6(a) and 6(b). Figure 6(a) was obtained in a measurement of a few hours performed about 1 h after the end of the activation. From the x-ray energy one can clearly identify the K_{α} contributions due to the decay of Ga and Zn isotopes. As one can see, the background level (not subtracted in this figure) is very small. Data corresponding to the same target, and collected over 2 weeks, about 2 months after the end of the activation are shown in Fig. 6(b) after background subtraction. As one can see, the contribution of the short lived Ga isotopes is no longer present, whereas by measuring for a sufficiently long period of time, the contribution of long lived Zn and Ge isotopes becomes evident.

X-ray energies characterize different elements but not different isotopes. However, in the present case, it was possible to discriminate isotopes by monitoring the activity of each element as function of time. An example is shown in Fig. 7 for Ga isotopes. One can clearly see two contributions due to the decay of ^{67}Ga($T_{1/2}=3.26$ days) and another shorter lived isotope. As shown in Fig. 7 the activity curve of Ga isotopes can be reproduced by assuming the simultaneous contribution of ^{67,68}Ga in agreement with CASCADE predictions. Following this procedure we unfolded the contributions of the different E.R. The residues produced have half lives ranging between 1 h and almost one year as shown in Table II. The activity of the long lived residues was monitored for about one year after the end of the experiment.

From the fits of the activity curves as a function of time we extracted, for each residue, the activity at $t=0$ (i.e., at the end of the activation run). Then, knowing the current incident on the target as function of time, the thickness of the different targets, the total x-ray detection efficiency, and the

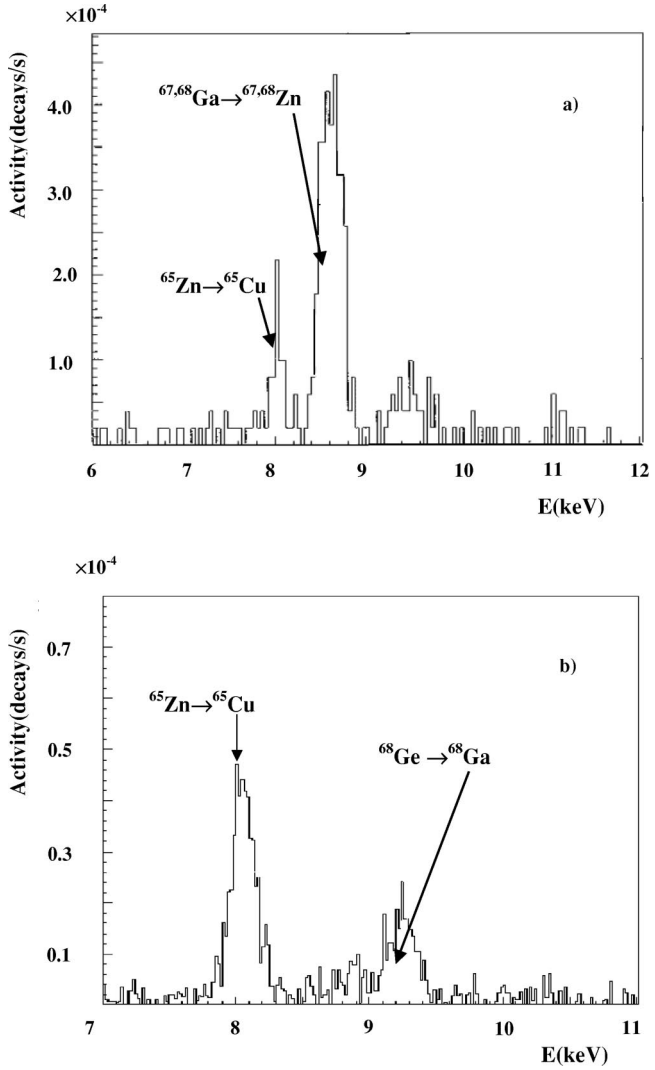

FIG. 6. (a) X-ray energy spectrum for the first target in the stack, measured 1 h after the activation run ended. The K_{α} lines of Zn and Ga isotopes are well above background. (b) X-ray energy spectrum for the first target in the stack, measured about one month after the activation run ended. The contribution of the short lived Ga isotopes is no longer evident.

K_{α} fluorescence probability [25] (the analysis was performed only on the K_{α} lines) we extracted the cross section for the production of each E.R.

The reaction ^{4}He+^{64}Zn was measured in the late 1950s and 1960s using a radiochemical method [26,27]. However these two data sets are not in agreement. Following the procedures discussed above, we analyzed our data for ^{4}He +^{64}Zn identifying the same E.R. found in Refs. [26,27], ^{67}Ge and ^{67}Ga, corresponding to the decay chains 1*n* and 1*p*, respectively, as also predicted by statistical model calculations. In our case the extracted fusion cross sections for ^{4}He +^{64}Zn are in good agreement with the data of Ref. [26].

For the reaction ^{6}He+^{64}Zn the identified heavy reaction products are the ones shown in Table II. Summing up the contribution of each nuclide we obtained the excitation function (open diamonds) shown in Fig. 8(a) compared with the excitation function for ^{4}He+^{64}Zn (closed triangles). The er-

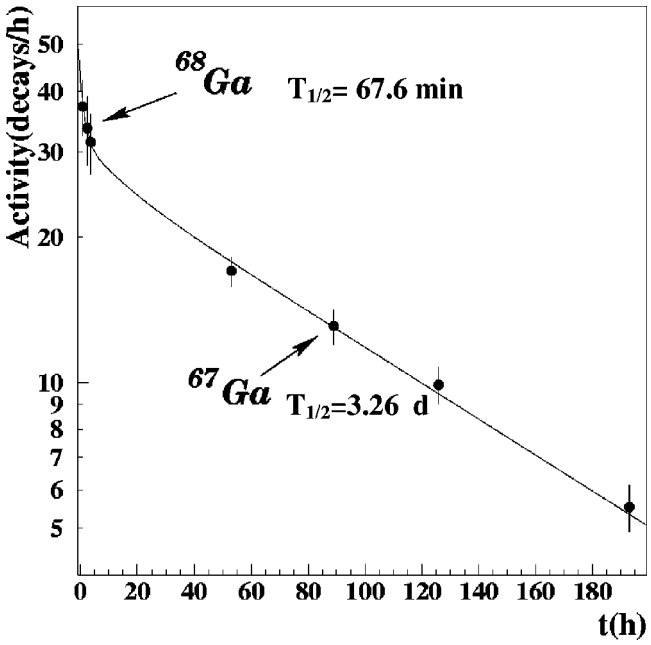

FIG. 7. Activity curve for Ga isotopes. The contributions of ^{68}Ga and ^{67}Ga can be disentangled due to their different half-life.

ror bars also include the contribution, calculated with CASCADE, of the stable E.R. not measured in the experiment. From this comparison a strong enhancement of the fusion cross section for the reaction induced by the halo nucleus ^{6}He is observed. However, by comparing, at all the energies explored, the cross sections for the production of each E.R. with the predictions of CASCADE, it is evident that the strong enhancement is mainly due to the contribution of a particular residue, i.e., ^{65}Zn. As an example in Fig. 9 we show the comparison between the CASCADE prediction and measured values at $E_{\mathrm{c.m.}}=10.55$ MeV, where the measured cross section for producing ^{65}Zn is the highest. A possible explanation for the much larger experimental yield of ^{65}Zn with respect to the calculated one is that other reaction mechanisms are contributing to this particular channel. Both, one and two neutron transfer could in fact produce ^{65}Zn. The two neutron transfer channel with its very high $Q_{\mathrm{g.s.}}$ could produce an excited ^{66}Zn* ($E^{*}=Q_{\mathrm{g.s.}}-Q_{\mathrm{opt}}$) which then decays by emitting light particles. One neutron emission from ^{66}Zn* will then produce ^{65}Zn. In Fig. 8(a) we also show the excitation function for ^{6}He+^{64}Zn where the measured ^{65}Zn contribution is replaced with the one calculated by CASCADE (closed diamonds). Comparing this excitation function with the one for the ^{4}He+^{64}Zn reaction a small enhancement of the fusion cross section for the ^{6}He induced collision appears to be present. However if one plots the fusion cross section as $\sigma/(\pi\times R^{2})$ versus $\mathrm{E_{c.m.}}/\mathrm{V_c}$, where R is the sum of the radii of projectile and target and V_{c} is the Coulomb barrier, the fusion excitation functions for the two systems appear to be very similar. This is shown in Fig. 8(b).

TABLE II. Different identified evaporation residues for the first target.

Residue	Decay chain	$T_{1/2}$
^{68}Ge	$2n$	271 day
^{68}Ga	$1p+1n$	67.6 min
^{67}Ga	$1p+2n$	3.26 day
^{65}Zn	$1\alpha+1n$	244 day

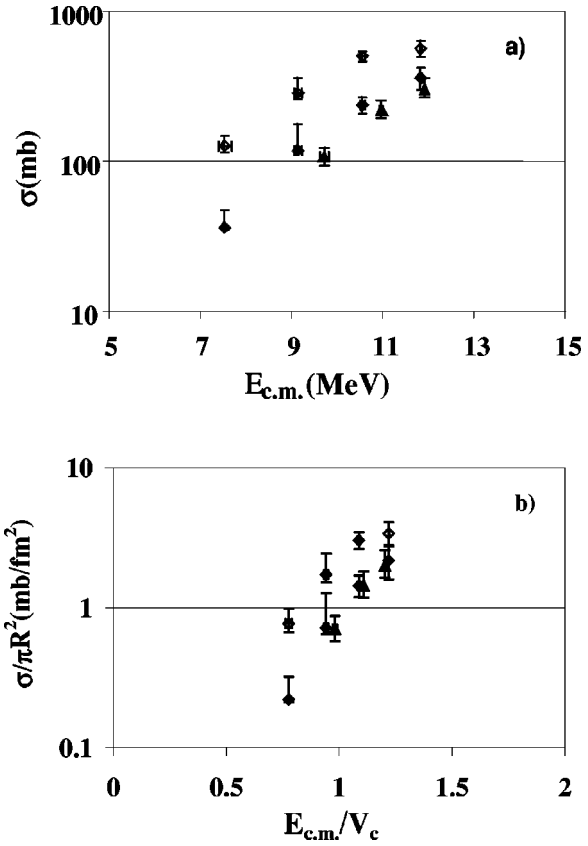

FIG. 8. (a) ^{6}He+^{64}Zn (open diamonds) and ^{4}He+^{64}Zn (triangles) excitation functions obtained by summing up the contribution of all measured heavy reaction products. The closed diamonds correspond to the excitation function obtained by substituting the measured ^{65}Zn contribution with the one calculated by CASCADE. (b) The same excitation functions have been plotted as $\sigma/(\pi\times R^{2})$ vs $E_{\mathrm{c.m.}}/V_{c}$. See text for details.

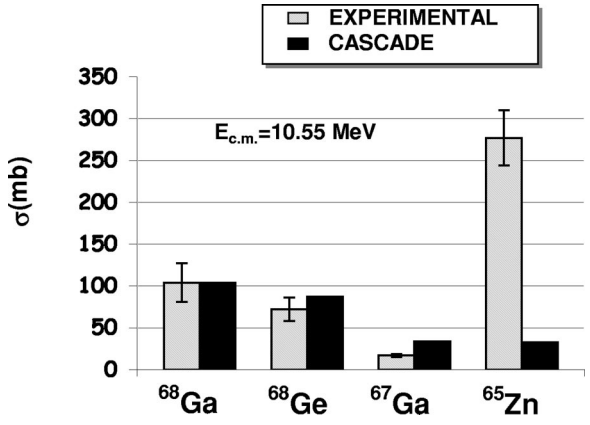

FIG. 9. Comparison of the experimentally measured cross sections of E.R. (dashed histogram) with the predictions of CASCADE (full histogram) at $E_{\mathrm{c.m.}}=10.55$ MeV.

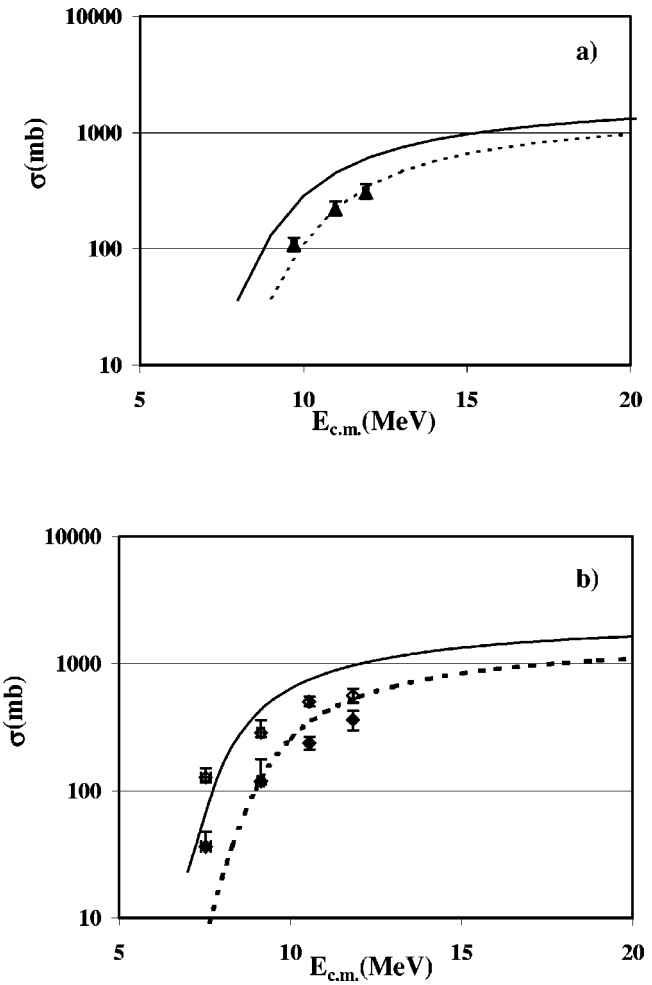

FIG. 10. (a) ^{4}He+^{64}Zn excitation function. Full line CCFULL calculations using the optical model potential parameters extracted from the elastic scattering. Dashed line, CCFULL calculations using a reduced r_0 value (see text). (b) ^{6}He+^{64}Zn excitation function. Open diamonds, experimentally measured excitation function. Closed diamonds, excitation function obtained by substituting the experimental ^{65}Zn contribution with the one calculated by CASCADE. Full line CCFULL calculations using the optical model potential parameters extracted from the elastic scattering. Dashed line, CCFULL calculations using a reduced r_0 value.

We would like to underline that the strong contribution of ^{65}Zn gives an apparently large enhancement of the cross section similar to the one measured by Trotta *et al.* for the system ^{6}He+^{238}U [9]. As discussed, we concluded that the strong enhancement observed in Fig. 8(a) is mainly due to transfer and not due to fusion. A new study of the ^{6}He +^{238}U reaction (performed by the same group as Ref. [9]) where a detector covering a larger angular range was used, showed that much of the fission cross section below the barrier was due to transfer/fission rather than fusion/fission [28] in agreement with the present result.

Coupled channel calculations using potential parameters, extracted from the elastic scattering analysis and the code CCFULL [29], were performed in an attempt to reproduce the fusion excitation functions for the systems ^{4}He+^{64}Zn and ^{6}He+^{64}Zn. We included in the calculations the coupling to the first excited state at $E^{*}=0.99$ MeV in the ^{64}Zn target and the coupling to the first excited state of the projectile in the ^{6}He induced reaction. As one can see in Figs. 10(a) and 10(b), such calculations overestimate the measured cross sections for both systems. By reducing the radius parameter from 1.2 fm to 1.0 fm a good agreement between the calculations and the experimental data are found. However, with such radius reduction, the elastic scattering data are not reproduced anymore (see Fig. 11) unless a very deep potential well is used ($V=340$ MeV). This is due to the previously mentioned Igo type ambiguities [23].

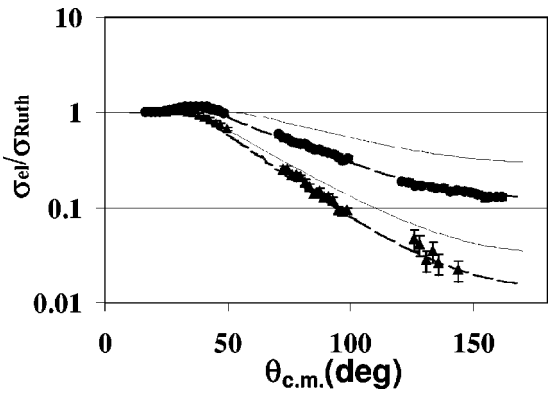

FIG. 11. Elastic scattering angular distributions as shown in Fig. 2(a). The dashed lines represent the result of the optical model fit, the full line represents the result of an optical model calculation where the parameters used are the ones showed in table I with the exception of r_0 where it was used $r_0=1.0$ fm.

IV. SUMMARY AND CONCLUSIONS

In this paper a complete study of the ^{4,6}He+^{64}Zn reactions has been performed to investigate the effects of the ^{6}He structure on the reaction mechanisms around the Coulomb barrier. Elastic scattering angular distributions were measured and the total reaction cross sections extracted by optical model analysis. The reaction cross section for the system ^{6}He+^{64}Zn was a factor of two larger than the one for the ^{4}He+^{64}Zn system measured at the same $E_{c.m.}$. The largest fraction of the total reaction cross section is due to direct processes such as transfer and breakup as found previously in the ^{6}He+^{209}Bi system [7].

The fusion excitation function was also measured using an activation technique. By detecting off-line the atomic x-rays following the E.R. decay we studied, for the first time, a fusion reaction induced by a light halo beam on a medium mass target. In the energy range explored in this experiment, a strong enhancement of the fusion cross section for ^{6}He induced reaction compared to ^{4}He induced reaction was observed. However, since the strong increase of the cross section is due only to the contribution of a particular reaction product ^{65}Zn, we concluded that other reaction mechanisms such as 1*n* and 2*n* transfer are contributing to the measured ^{65}Zn cross section. An excitation function, where the measured ^{65}Zn contribution was replaced by the one calculated with the statistical code CASCADE, does not show an enhancement with respect to the one for the ^{4}He induced col-

lision. A new experiment is currently planned to extend the energy range of the measured excitation function. The data presented clearly show that the off-line detection of x-rays following E.R. decay is a useful "tool" for studying fusion reactions induced by light halo nuclei on medium mass targets.

ACKNOWLEDGMENTS

The authors wish to thank Professor G. Pappalardo and Professor E. Gadioli for supplying the Si(Li) detectors and the detector shields used in the off-line x-ray measurements and Dr. K. Hagino for providing the computer code CCFULL. Thanks are also due to all the technical staff of the Centre de Recherches du Cyclotron at Louvain-la-Neuve for their help during the setting up of the experiment and the production of ^{6}He beam. This work has been partially financed by UK EPSRC and the European Community-Access to Research Infrastructure action of the Improving Human Potential Programme, Contract No. HPRI-CT-1999-00110 and the Belgian program P5/07 on interuniversity attraction poles of the Belgian-State Federal Service for Scientific, Technical, and Cultural Affairs.

[1] M. C. S. Figueira *et al.*, Phys. Rev. C **46**, 1139 (1992).
[2] L. C. Canto *et al.*, Phys. Rev. C **52**, R2848 (1995).
[3] L. C. Canto *et al.*, Phys. Rev. C **58**, 1107 (1998).
[4] K. Hagino *et al.*, Phys. Rev. C **61**, 037602 (2000).
[5] P. A. De Young *et al.*, Phys. Rev. C **58**, 3442 (1998).
[6] J. J. Kolata *et al.*, Phys. Rev. Lett. **81**, 4580 (1998).
[7] E. F. Aguilera *et al.*, Phys. Rev. Lett. **84**, 5058 (2000).
[8] E. F. Aguilera *et al.*, Phys. Rev. C **63**, 061603(R) (2001).
[9] M. Trotta *et al.*, Phys. Rev. Lett. **84**, 2342 (2000).
[10] J. L. Sida *et al.*, Nucl. Phys. **A685**, 51c (2001).
[11] C. Signorini *et al.*, Eur. Phys. J. A **2**, 227 (1998).
[12] A. Youshida *et al.*, Phys. Lett. B **389**, 457 (1996).
[13] C. Signorini *et al.*, Eur. Phys. J. A **13**, 129 (2002).
[14] M. Dasgupta *et al.*, Phys. Rev. Lett. **82**, 1395 (1999).
[15] R. J. Woolliscroft *et al.*, Phys. Rev. C **68**, 014611 (2003).
[16] J. J. Kolata, Eur. Phys. J. A **13**, 117 (2002).
[17] S. B. Moraes *et al.*, Phys. Rev. C **61**, 064608 (2000).
[18] T. Davinson *et al.*, Nucl. Instrum. Methods Phys. Res. A **454**, 350 (2000).
[19] J. F. Ziegler and J. P. Biersack, SRIM, program version srim-2000.40, 2000.
[20] M. Cabibbo. PhD thesis, Universita' di Catania, 1998.
[21] M. J. Rhoades-Brown *et al.*, Phys. Rev. C **21**, 2417 (1980).
[22] A. Di Pietro *et al.*, Europhys. Lett. **64**, 309 (2003).
[23] G. Igo, Phys. Rev. **115**, 1665 (1959).
[24] F. Pühlhofer, Nucl. Phys. **A280**, 267 (1977).
[25] National Nuclear Data Center, Brookhaven National Laboratory, Upton, NY, 2003.
[26] N. T. Porile, Phys. Rev. **115**, 939 (1959).
[27] F. H. Ruddy and B. D. Pate, Nucl. Phys. **A127**, 305 (1969).
[28] R. Raabe (unpublished).
[29] K. Hagino *et al.*, Comput. Phys. Commun. **123**, 143 (1999).